TECHNICAL MEMORANDUM

509

A revised formulation of ocean wave dissipation and its model impact.

Jean-Raymond Bidlot, Peter Janssen and Saleh Abdalla

Research Department

January 2007

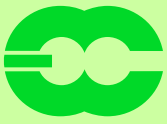

European Centre for Medium-Range Weather Forecasts
Europäisches Zentrum für mittelfristige Wettervorhersage
Centre européen pour les prévisions météorologiques à moyen terme

Series: ECMWF Technical Memoranda

A full list of ECMWF Publications can be found on our web site under:
http://www.ecmwf.int/publications/

Contact: library@ecmwf.int

European Centre for Medium-Range Weather Forecasts
Shinfield Park, Reading, RG2 9AX, England

Abstract

The wave model dissipation source function in the ECMWF operational model has been reformulated in terms of mean wave parameters that give more emphasis on the high-frequency part of the wave spectrum resulting in a more realistic interaction between windsea and swell. This has allowed the relaxation of the prognostic frequency range over which the model equations are integrated. These modifications resulted in improved analyses of wave model parameters, particularly those that are more sensitive to the high frequency part of the spectrum (e.g. mean wave period). Following pre-operational testing, the changes were implemented in the operational model in April 2005. Long term statistics confirm the benefit of the revised formulations.

1 Introduction

ECMWF produces twice daily analyses and forecasts of the sea state over the world oceans. The physics of the wave model is based on WAM Cycle 4, which became available in 1991. The ever- changing operational environment required further developments, such as massive parallel processing, to be incorporated in the wave model. Furthermore, there were numerical improvements in the advection scheme, in the time-integration scheme and in the determination of the wave stress. The ECMWF version of the WAM model will therefore be called 'ECWAM'. In its current global configuration ECWAM is two-way coupled to the atmospheric model and altimeter and ASAR data are assimilated to produce the wave analysis. It is run in all forecasting systems in use at ECMWF, from deterministic and probabilistic 10 day forecasts, to monthly and seasonal time scales. The latest developments have been summarized in Janssen *et al.* (2005) and Janssen (2004).

ECMWF continuously works at monitoring and improving the quality of its products. In this respect, verification against observations is essential. Recently, the usual comparison against buoy wave height data has been extended to include buoy wave spectra (Bidlot *et al.*, 2005b). This novel approach has revealed a number of problems with the model (and the associated atmospheric model). In this paper, it is shown that the original ECWAM formulation of the dissipation due to whitecapping is not entirely adequate when both windsea and low frequency swell are present. We also show why the dynamic range of the model had to be extended. This was achieved following several model changes centred around the reformulation for wave dissipation due to whitecapping. Indeed, by comparing model and buoy spectra, it became apparent that under light wind conditions, in the presence of low-frequency swell, there were often cases where there were no locally generated wind waves (windsea). Although this was a relatively minor problem in terms of significant wave height, it affected the quality of wave parameters that are based on higher moments of the wave spectrum such as the mean period. At the same time, users of ECMWF wave products reported issues with the mean period as pointed out by Kumar *et al.* (2003) and by Steve Barstow (private communication, 2004). A practical solution was quickly found as described below.

Note that there are earlier references to the deficiencies of WAM when windsea is generated in the presence of swell (Tolman and Chalikov, 1996, and Booij and Holthuijsen, 2002). The benefits of the revised formulation were demonstrated prior to its operational implementation (Bidlot et al., 2005). This encouraged other wave modellers to try it in their wave model configuration. Ardhuin reported on the positive impact of the new formulation when it was incorporated into his version of WAVEWATCH III (Ardhuin, 2005, and Ardhuin *et al.*, 2007). Osuna *et al.* (2006) tested as well some of these changes in their version of WAM (ProWAM) for the study of wind and wave modelling in the Irish Sea. They found that the new formulation had limited impact on the wave hindcasts; however no proper assement was provided. In this paper, we show that the new version of ECWAM has improved in many aspects.

The layout of the paper is as follows. The old and new formulations are described in Section 2. Simple examples on how the revised formulation compares to the old one are given in Section 3. The new configuration of the

model was tested both in stand-alone mode (i.e. uncoupled to the atmospheric model) and in the coupled configuration prior to its operational implementation as presented in Section 4. The impact on the quality of the operational model since implemetation is discussed in Section 5. A detailed description of the wave data used for verification is given in the Appendix.

2 A revised version of wave dissipation

In ECWAM dissipation due to whitecapping, S_{ds}, used to be modelled in the manner first suggested by Hasselmann (1974) and later extended by Janssen (Komen *et al.*, 1994).

Introduce the mean frequency $\langle\omega\rangle$ by means of the inverse mean frequency,

$$\langle\omega\rangle = \int d\vec{k}\, F(\vec{k}) / \int d\vec{k}\, F(\vec{k})/\omega \tag{1}$$

with $F(\vec{k})$ the wavenumber spectrum, $\vec{k}$ the wavenumber and ω the angular frequency. A similar relation for the mean wavenumber $\langle k\rangle$ is

$$\sqrt{\langle k\rangle} = \int d\vec{k}\, F(\vec{k}) / \int d\vec{k}\, F(\vec{k})/\sqrt{k}. \tag{2}$$

Hasselmann (1974) suggested the following quasi-linear dissipation source function

$$S_{ds} = -\gamma_d F, \tag{3}$$

with

$$\gamma_d = \beta\langle\omega\rangle\, s^{2m} \left[(1-a)\frac{k}{\langle k\rangle} + a\left(\frac{k}{\langle k\rangle}\right)^2\right], \tag{4}$$

where the mean steepness s is defined as

$$s^2 = \langle k\rangle^2 \int d\vec{k}\, F(\vec{k}) \tag{5}$$

Here, β, a and m are constants which still need to be determined. Note that in the original work of Hasselmann (1974) the second term in the square bracket was absent ($a = 0$). The reason for this is that Hasselmann assumed a large separation between the length scale of the waves and the whitecaps, giving a dissipation term with a linear dependence on the wavenumber. For the high-frequency part of the wave spectrum, however, such a large gap between waves and whitecaps may not exist, therefore allowing the possibility of a different dependence of the dissipation on wavenumber.

The first rational attempt to determine the unknown coefficients in the dissipation source function was reported by Komen *et al.* (1984). These authors started from the empirical expression for wind input of Snyder *et al.* (1981), which was adapted to accomodate friction velocity scaling, whilst the exact form of Hasselmann's nonlinear transfer was taken. For a constant wind speed, the energy balance equation was integrated until stationary conditions were reached, and the unknown coefficients m and β were chosen in such a way that the equilibrium spectrum resembled the Pierson-Moskovitz (1964) spectrum as closely as possible (Note that in their work a was put to zero from the outset). The power m was found to be equal to 2 while the coefficient β was of the order of 3.

Later, Janssen (see Komen *et al.*, 1994) introduced a wind input source function based on Miles theory, which resulted in much higher inputs at higher frequencies. Consequently, the dissipation source function required some adaptation, in particular at higher frequencies. He fixed m to 2 and reached, using the discrete interaction approximation (DIA) to the nonlinear transfer, optimal results with $a = 0.5$ and $\beta = 4.5$.

Note that the linear dependence of the dissipation source term on the spectrum itself, as expressed in (3), has recently received experimental backing following a field experiment carried out at Lake George where extreme wave breaking condition have been observed (Young and Babanin, 2006). Also, from the dissipation source function an estimate of the whitecap fraction can be obtained (Kraan *et al.*, 1996). Using Eq. (3-4) it is found that the whitecap fraction is proportional to s^{2m}. Using video cameras, Kraan *et al. (1996)* and Lafon *et al.* (2004) found that the unknown parameter m is about 2.

Inspecting Eqns. (2) and (5), it is apparent that the mean steepness and mean frequency parameters used in the above parametrization of the dissipation are to a considerable extend determined by the low frequency part of the spectrum (swell) rather than by the windsea part of the spectrum. This has, as discussed shortly, undesirable consequences when both swell and windsea are present.

In the new version of ECWAM, wave dissipation due to whitecapping, S_{ds}, is still modelled in the manner suggested by (4). However, the mean wave number $\langle k \rangle$ and mean frequency $\langle \omega \rangle$ are defined using weighted spectral integrals that put more emphasis on the high frequencies.

Introduce the mean angular frequency $\langle \omega \rangle$ by means of the first ω-moment of the spectrum,

$$\langle \omega \rangle = \int d\vec{k}\, \omega F(\vec{k}) / \int d\vec{k}\, F(\vec{k}) \tag{6}$$

A similar relation for the mean wavenumber $\langle k \rangle$ is also used,

$$\sqrt{\langle k \rangle} = \int d\vec{k}\, \sqrt{k} F(\vec{k}) / \int d\vec{k}\, F(\vec{k}) \tag{7}$$

and the mean steepness s is defined as in (5). The dissipation source function is still modelled as in (3) and (4), where m is equal to 2, and β and a are two constant parameters to be determined.

Another point of concern is the choice of the maximum value of the prognostic frequency range. The wave model spectrum is discretized between a minimum (f_{min}) and maximum frequency (f_{max}), however, because of limitations due to the numerics and the assumptions made on the model source terms, the equations are only integrated up to a cut-off prognostic frequency. For frequencies above this cut-off frequency, ECWAM enforces a diagnostic f^{-5} spectral shape. Since July 1999, the ECWAM model defines this prognostic range as all frequencies f which satisfy

$$f_{min} \leq f \leq \min(2.5\langle f \rangle, f_{max}) \tag{8}$$

where f_{max} is the maximum discretized frequency ($f_{max} \simeq 0.41 Hz$ for 25 frequencies and 0.54 Hz for 30 frequencies) and $\langle f \rangle = \langle \omega \rangle / 2\pi$. It replaced the previous definition of the original WAM Cycle 4, where the upper prognostic frequency was given by $\min(\max(2.5\langle f \rangle, 4 f_{PM}), f_{max})$ (with f_{PM} the Pierson-Moskovitz frequency). In 1999, this change had a favourable impact on relations such as the mean square slope versus wind speed. Also, when compared to ERS-2 altimeter wave height data, the first-guess wave height error reduced by 5%. However, under light wind conditions in the presence of low-frequency swell, we found that the local windsea was not generated or seriously delayed in its growth. This lack of wave growth at high frequency was identified to be the consequence of the imposition of the diagnostic frequency tail at that range, effectively wiping out windsea energy at high frequencies. Therefore, it was thought to be desirable to increase the upper limit in order to capture windseas in light wind situations. This should be done, however, in such a way that relations such as

mean square slope and Charnock parameter versus wind speed do not suffer (to avoid undesirable effects when coupled to the atmospheric model as pointed out by Janssen 2004). Also, the choice of this upper limit should not be influenced by the presence of low frequency swell.

In the new version of ECWAM we have replaced in Eq.(8) the mean frequency of the total sea by the mean frequency of the wind sea only, denoted by f_{meanWS}. Namely,

$$f_{min} \leq f \leq \min(2.5 f_{meanWS}, f_{max}) \tag{9}$$

where f_{meanWS} is the mean frequency based on the ω^{-1} moment (Eq.(1)) but only for spectral components that satisfy

$$S_{input} > 0. \quad or \quad \frac{28}{c} u_* \cos(\Delta\theta) \geq 1. \tag{10}$$

where S_{input} is the wind input source term, c is the wave phase speed, u_* is the friction velocity and $\Delta\theta$ is the difference between the wind direction and the wave propagation direction. Note that Eq.(1) was used because it gave stable estimates of the windsea mean frequency.

A tuning exercise was performed in such a way that the duration limited growth curve for significant wave height and the time evolution of the Charnock parameter resembled as much as possible the corresponding results of the reference model (which is essentially WAM Cycle 4, but using Eq. (8)). As a result we found that

$$\beta = 2.1, \; a = 0.6, \text{ and } \hat{\alpha} = 0.0095 \tag{11}$$

where $\hat{\alpha}$, is a constant that controls the asymptotic value of the Charnock parameter α.

$$\alpha = \hat{\alpha} / \sqrt{1 - \tau_w / \tau} \tag{12}$$

where τ is the total stress and τ_w the wave induced stress.

A few other numerical adjustments were also necessary. By analysing simple wave growth cases, we found that for light winds the Hersbach-Janssen limiter (1999) to the wave growth

$$|\Delta F|_{max} = 510^{-7} g u_* f^{-4} \langle f \rangle \Delta t \tag{13}$$

was not sufficiently controlling the growth (i.e. there were signs of unstable growth). It was reduced by a factor of 0.6 and $\langle f \rangle$ was replaced by f_{meanWS} to remove the dependence of the limiter on the presence of low frequency swell.

Finally, it had been known for a while that more accurate results could be obtained if the total stress look-up table that relates the wind speed and the wave induced stress τ_w was expressed in terms of $\sqrt{\tau}_w$ instead of τ_w. This was implemented in the new operational version of ECWAM.

Note also that since the introduction of the coupling between WAM and the atmospheric model, several modifications to the numerics were made to improve the calculation of the surface roughness over the oceans as determined by the Charnock relation (Janssen 2004). These changes have also benefitted the uncoupled version of ECWAM. Firstly, the integration of the source terms has been made fully implicit, and moreover, the wave stress and total stress are updated following the update of the spectrum before the integration is continued. This change is relevant for rapidly changing wind fields (Janssen and Bidlot, 2001). Secondly, the accuracy of the numerical evaluation of the integral for the high frequency contribution to the wave induced stress was improved (Bidlot and Janssen, 2003). Furthermore, the maximum value for the Charnock parameter in the wave stress table was changed to 0.2 and the number of entries in the table was doubled. Finally, the accuracy of the total stress table was also increased by doubling the number of entries in both dimensions. The coupled version of ECWAM does however benefit further from a more frequent update of the wind (every time step) and also from improvements such as the use of variable air density, gustiness (Abdalla *et al.*, 2003) and neutral wind forcing (Bidlot and Janssen, 2003).

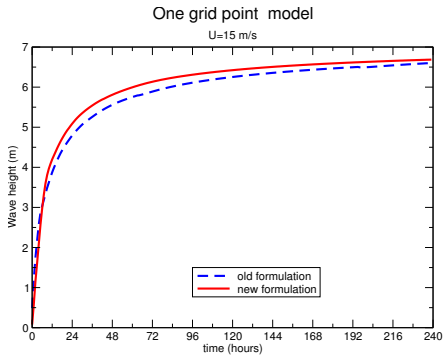

Figure 1: Time evolution of wave height for the one grid point model over a 10-day period when forced by steady 15 m/s wind. The integration time step is 900 s.

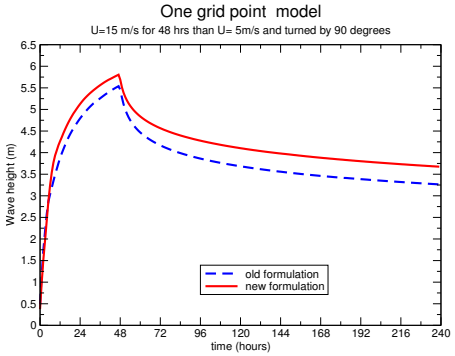

Figure 2: Time evolution of significant wave height over a 10-day period for the one grid point model. Initially the wind speed is 15 *m/s, and after* 48 *hrs it drops to 5 m/s while the wind direction turns by* 90°.

3 Results for simple test cases

In Figure 1 the duration-limited growth curve from the new version of ECWAM is compared with results from the old version. The agreement is satisfactory, but it cannot be perfect for the following reasons: for short times the growth limiter is more effective in the new model configuration resulting in lower growth. In addition, with the new definition of mean wavenumber, the mean steepness s is more sensitive to changes in the wave spectrum. As waves get smoother in the course of time the amount of dissipation reduces more quickly in the new set up. Consequently, there is a slightly faster growth after the inital stage of wave growth before leveling off to a similar level at saturation for large times. For strong winds, the saturation in wave height only plays a role for very long duration, hence it is expected that extreme sea states will be enhanced by this change. For light winds no changes are expected because saturation already occurs in less than one day.

In the next experiment swell decay is compared. The one grid point model was run for 2 days with a steady wind of 15 m/s, after which the wind speed dropped to 5 m/s while the wind direction turned by 90°. Results for wave height are shown in Figure 2. Decay time scales in the new setup are slightly longer because the dissipation source function is a more sensitive function of the sea state.

The final set of idealized experiments were performed to investigate the impact of the presence of low-frequency swell on the growth of windsea. The swell spectrum had a mean direction 90° to the right of the wind direction while its peak frequency was 0.045Hz and the mean steepness of the swell system was of the order 0.03. The wind speed was 10 m/s. With the definition of prognostic range given in Eq. (8), no windsea is generated as the prognostic frequency range is too narrow to capture the yound windsea. Hence no comparison is possible

and we therefore compare results when the wider frequency range of the original WAM Cycle 4 is used. In that case, at the early stages windsea is generated but it does not grow as fast as without swell (Figure 3 a). This behaviour was found to be connected to the old definition of the mean frequency in the growth limiter (13). In the presence of swell, $\langle f \rangle$ is reduced and the limiter becomes too strict, slowing down the initial growth of the windsea. At later stages (Figure 3 b,c,d), the windsea in the presence of swell becomes much larger than in the absence of swell. This was however not the intention of the original WAM development and has no observational basis. In general cases over the oceans, windsea growth should not be significantly influenced by the presence of a gentle swell (Ardhuin et al. 2007). The reason for the too large windsea growth in the presence of swell is the old computation of the mean wave steepness which gives a considerable emphasis on the low frequencies. The new formulation, with Eq. (9), i.e. the use of f_{meanWS} in the dissipation and in the limiter, leads to the interaction of windsea and swell as shown in Fig. 4. The new setup gives a satisfactory qualitative behaviour of the interaction of windsea and swell since the windsea grows at almost the same rate with or without the presence of swell.

4 Real case assessements

4.1 Stand-alone runs

The initial testing of the new formulation was done in the context of stand-alone ECWAM hindcasts. In this configuration, ECWAM is forced by 6-hourly analysed 10-m winds without wave data assimilation and no coupling with the atmospheric model. The runs were performed with the 0.5° (55 km) version of the model. An example of the impact of the new formulation in terms of the mean difference (new-old) for significant wave height (H_s) and mean wave period (T_z) for a boreal winter (Dec. 2003) is shown in Figure 5 and another example during a Northern Hemisphere summer (July 2004) is shown in Figure 6. Areas with substantial differences are apparent, especially for T_z. With the new formulation, wave heights are larger in the storm tracks (active generation), whereas they are smaller in the Tropics (swell condition). Mean periods are much reduced, in particular around India (Figure 5), and both in the eastern tropical Pacific and Atlantic. These areas have a sea state that is a combination of a dominant swell and high-frequency windsea. These conditions are better modelled by the new formulation. During the Northern Hemisphere summer (Figure 6), the north Pacific is also dominated by swell accompanied with short fetch/duration storms and some reduction in wave height occurs.

These hindcasts were compared to all available wave observations (see the appendix for details). A global verification with altimeter wave heights from ENVISAT and Jason is presented in Table 1. For all ocean basins combined, there is a reduction in scatter index for both seasons and hardly no change to the global bias, which is still slightly negative. In the Tropics, the scatter index is also nicely reduced with a small bias that becomes negative.

Buoy wave data were also used for validation. The coverage is not global and mainly representative of Northern Hemisphere coastal areas (especially before the end of 2004, see the appendix for details), but the advantage is that the comparison can also be made in terms of wave periods. Table 2 confirms the improvement in terms of wave heights. It also shows the marked gain in terms of mean wave period. There is however a slight deterioration of the peak period statistics. The worsening of the peak period statistics is probably caused by the increased variability of the modelled sea state due to the inclusion of high-frequency windseas in the new set up.

A good insight into the nature of this under/over estimation can be obtained by comparing the wave model spectra with buoy 1-D spectra. This comparison is however limited to the American and Canadian coastal areas including Hawaii and a buoy off Christmas Island in the equatorial Pacific. Nevertheless, as shown in Figure 7,

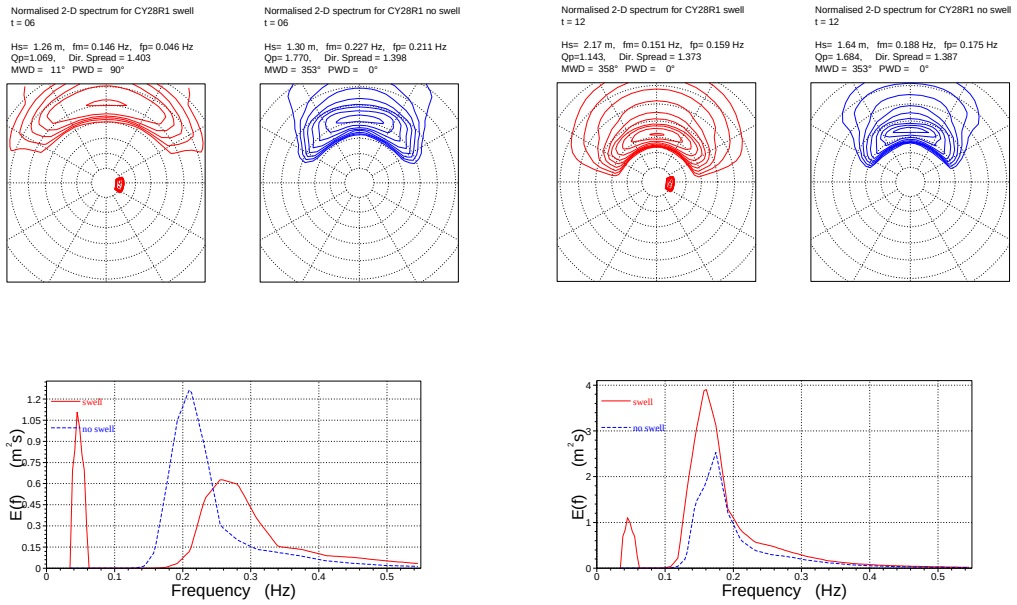

(a) t= 6 (b) t=12

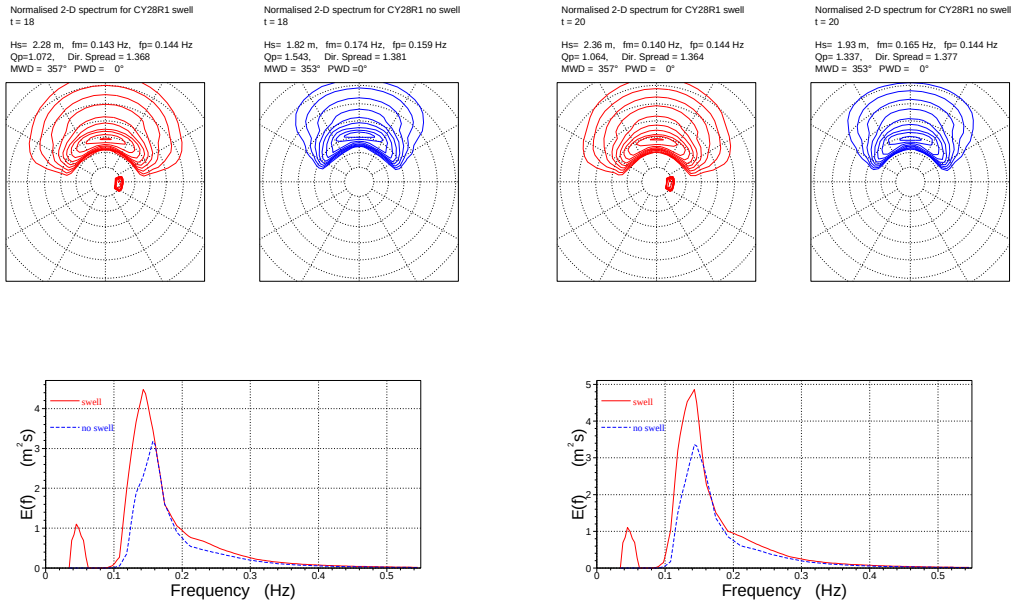

(c) t=18 (d) t=24

Figure 3: Time evolution of one grid point model 2-D and 1-D spectra in the presence of swell (in red) or not (in blue) for the old model but with the upper prognostic frequency of the original WAM Cycle 4 ($\min(\max(2.5\langle f\rangle, 4f_{PM}), f_{max})$*). In the presence of such swell, the old ECWAM setup does not give any growth of windsea and is not shown. The wind speed is constant at* 10 *m/s. The spectra are shown every 6 hours for a day from the start. For each time, the 2-D spectra are plotted using the same 10 contour levels that are chosen between the minimum and the maximum values of both cases. The concentric circles in the polar plots are spaced every 0.05 Hz.*

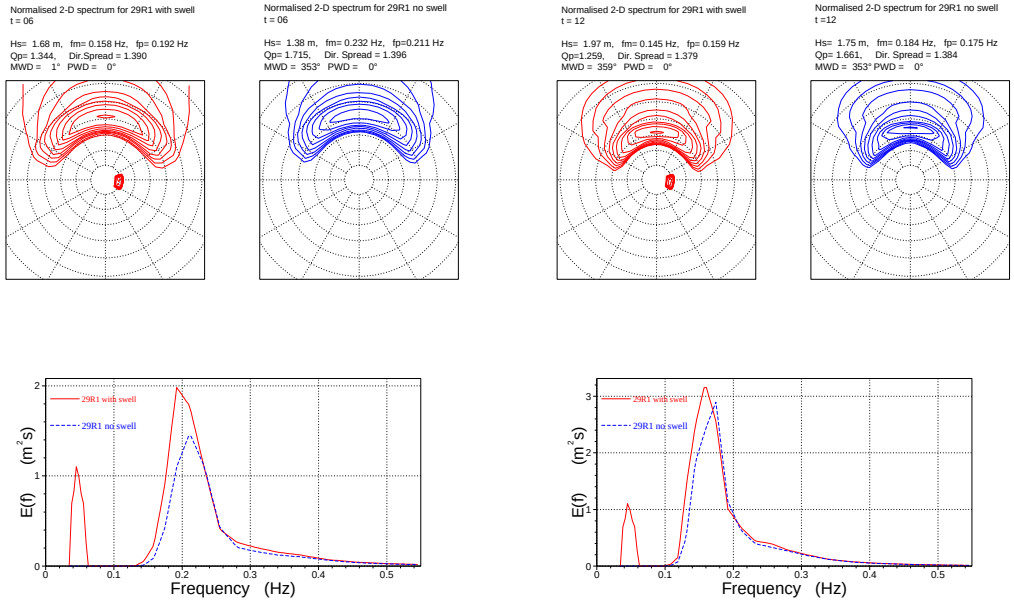

(a) t= 6 (b) t=12

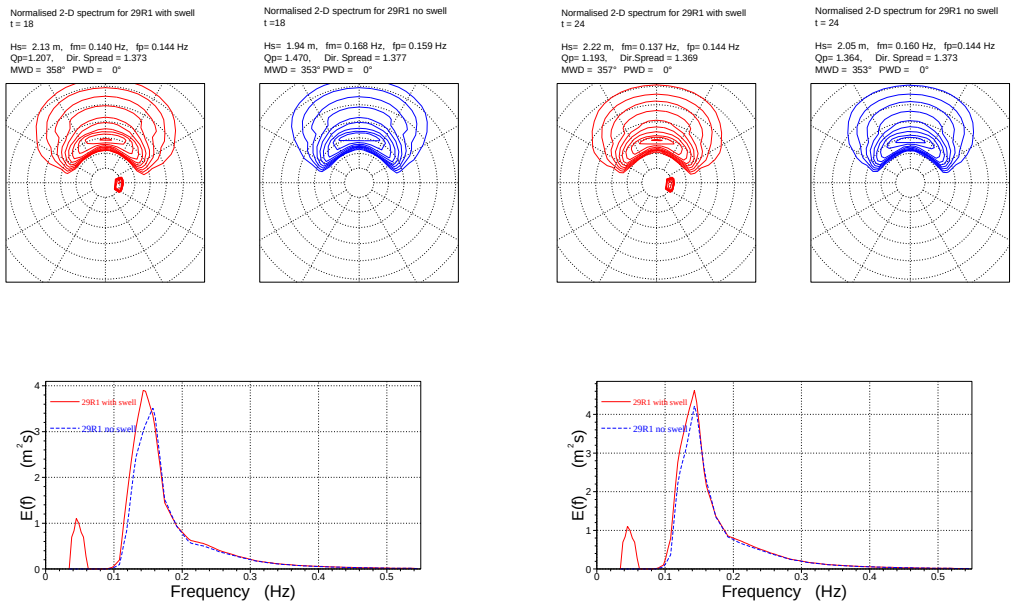

(c) t=18 (d) t=24

Figure 4: Time evolution of one grid point model 2-D and 1-D spectra in the presence of swell (in red) or not (in blue) for the new model. The wind speed is constant at 10 *m/s. The spectra are shown every 6 hours for a day from the start. For each time, the 2-D spectra are plotted using the same 10 contour levels that are chosen between the minimum and the maximum values of both cases. The concentric circles in the polar plots are spaced every 0.05 Hz.*

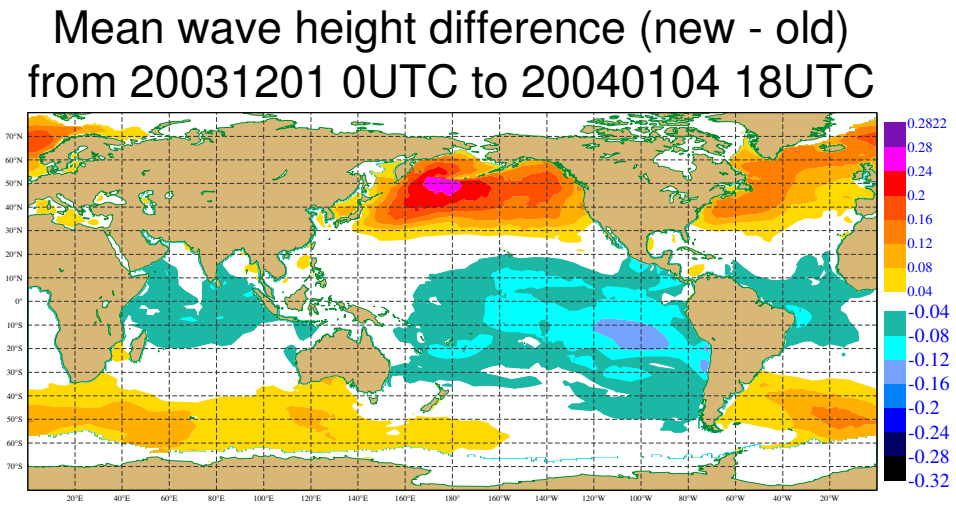

(a) wave height (m)

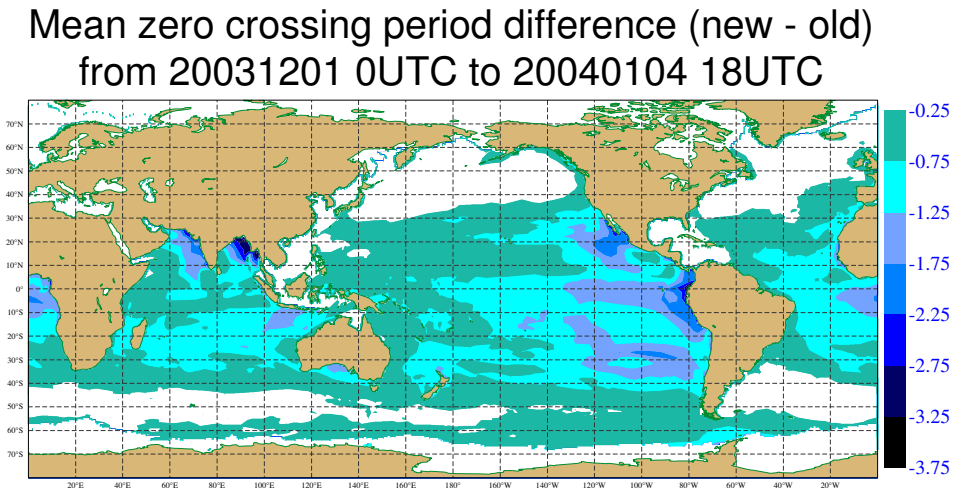

(b) mean wave period (s)

Figure 5: Mean difference (new-old) for December 2003 for stand-alone 0.5° *hindcasts without any data assimilation. Colour shading is only used if the absolute difference is larger than 4 cm for wave heights and 0.25 s for mean periods.*

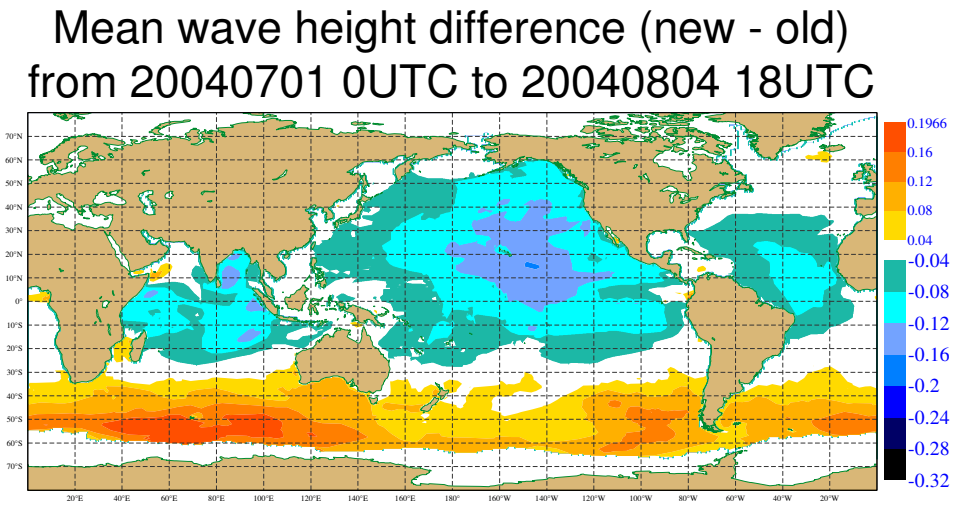

(a) wave height (m)

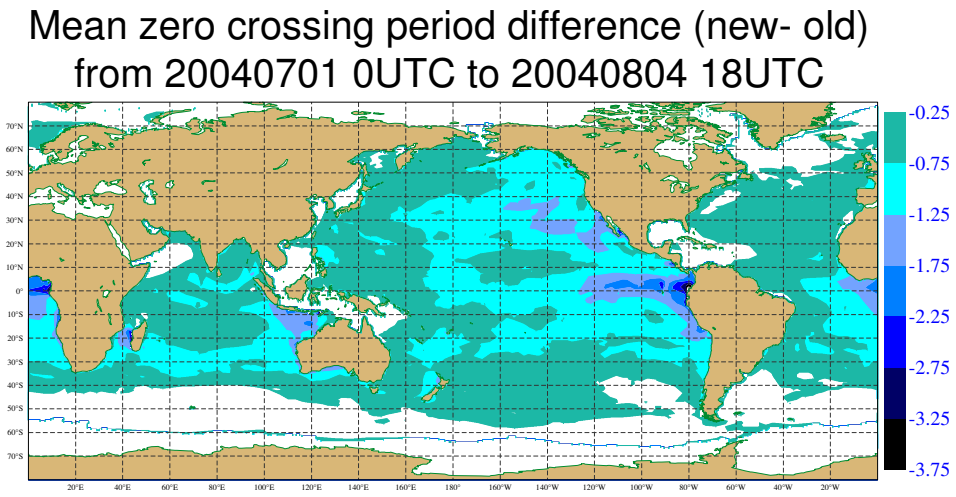

(b) mean wave period (s)

Figure 6: Mean difference (new-old) for July 2004 for stand-alone 0.5° *hindcasts without any data assimilation. Colour shading is only used if the absolute difference is larger than 4 cm for wave heights and 0.25 s for mean periods.*

Table 1: Verification of the stand-alone 0.5° *hindcasts with altimeter wave heights for December 2003 (winter) and July 2004 (summer). No data assimilation was performed for the hindcasts. Operational analysis winds were used to force ECWAM. The old formulation (old) is compared to the new one (new) in terms of scatter index (standard deviation of the difference normalised by the mean of the observations) and bias (model-altimeter). Bias corrected altimeter super-observations were used (see the appendix). Tropics are defined as the area between* $\pm 20^\circ$.

Comparison with altimeter wave heights : S.I.(%) [bias(m)]				
data source	old (winter)	new (winter)	old (summer)	new (summer)
ENVISAT global	15.28 [-0.05]	14.43 [-0.04]	13.75 [-0.08]	13.29 [-0.08]
Jason global	16.73 [-0.06]	15.53 [-0.05]	15.25 [-0.06]	14.16 [-0.06]
ENVISAT Tropics	14.66 [0.01]	13.75 [-0.04]	12.31 [-0.04]	11.80 [-0.09]
Jason Tropics	15.87 [0.03]	14.83 [-0.02]	13.62 [0.03]	13.20 [-0.03]

Table 2: Verification of the stand-alone 0.5° *hindcasts with buoy data for December 2003 (winter) and July 2004 (summer). No data assimilation was performed for the hindcasts. Operational analysis winds were used to force ECWAM. The old formulation (old) is compared to the new one (new) in terms of scatter index (standard deviation of the difference normalised by the mean of the observations) and bias (model-buoy) for wave height (H_s), mean period (T_z) and peak period (T_p). The buoy data were either obtained from the operational archive (GTS) or derived from 1D buoy spectra obtained from NDBC and MEDS (see the appendix).*

Comparison with buoy data : S.I.(%) [bias (m or s)]				
data source	old (winter)	new (winter)	old (summer)	new (summer)
H_s	16.94 [-0.35]	15.99 [-0.27]	21.28 [0.01]	19.91 [-0.02]
T_z	12.46 [-0.16]	10.86 [-0.44]	16.96 [-0.01]	11.66 [-0.17]
T_p	15.76 [-0.23]	16.06 [-0.04]	27.56 [0.42]	29.47 [0.46]

it indicates that the old formulation underestimates wave energy at high frequencies (the windsea part of the spectrum). This is still true if the buoy network is split per ocean basin. For winter months, the underestimation is also present at all frequencies. For summer months, especially with the old formulation, the model largely overestimates swell at around 12 seconds. This is most pronounced in the northeastern Pacifici (not shown). As expected, the new formulation does indeed improve the prediction of windsea and also reduces the swell overestimation of the summer months at around 10-15 seconds. Note however, that it does not improve the model fit to the data for very long-period swell (above 18 s in summer time). Figure 7 also indicates that the new formulation has positive impact on the standard deviation of the difference except for low frequency range in the summer case.

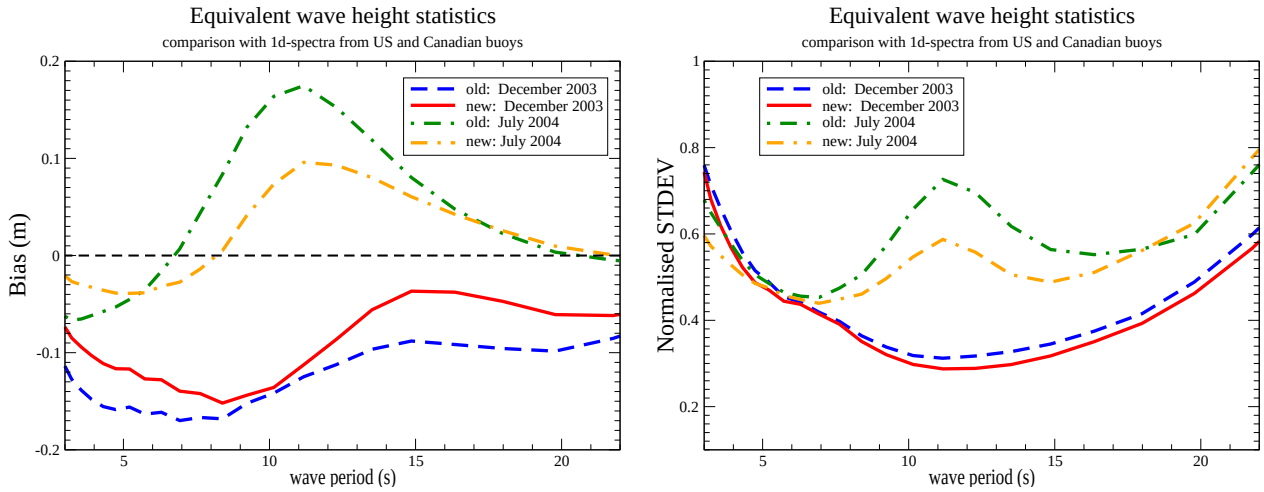

(a) BIAS(model-buoy) (m)

(b) Normalised STDEV

Figure 7: Comparison between wave model hindcasts with the new and the old formulation and 1-D wave spectra for locations along the American and Canadian coasts for December 2003 and July 2004. The spectral data were smoothed by averaging over 3 consecutive wave model frequency bins and by converting the average energy density to equivalent wave heights. The different statistics are then plotted in terms of the corresponding wave period of each wave model frequency bin at mid point. All runs used the stand-alone 55km model without any data assimilation. The normalised standard deviation of the difference (STDEV) is computed by normalising with the standard deviation of the observations for each frequency bin.

4.2 Coupled runs

The new formulation is also beneficial on the two-way coupling with the atmosphere. The feedback of the waves on the winds is modelled via a wave dependent Charnock parameter which enters in the formulation of the surface roughness used to determine the atmospheric surface stress over the ocean (Janssen, 2004). Figure 8 displays the mean Charnock parameter as a function of the 10-m wind speed. The old formulation with the original WAM Cycle 4 prognostic frequency range (green squares) had a tendency to result in too high values of the Charnock parameter around 10 m/s. This led to the introduction of the previous prognostice range (blue circles) (Bidlot *et al.*, 1999). Successive changes to the model (Janssen and Bidlot, 2001, Abdalla *et al.*, 2003, Bidlot and Janssen, 2003, Janssen, 2004 and Janssen *et al.*, 2005) have reduced the mean Charnock parameter to levels below the values obtained from the HEXOS data (Smith *et al.*, 1992.). On the other hand, the new formulation (red triangles) yields mean levels for the Charnock parameter that are comparable to the mean HEXOS data. The mean Charnock parameter is also less noisy for low wind speed around 5 m/s.

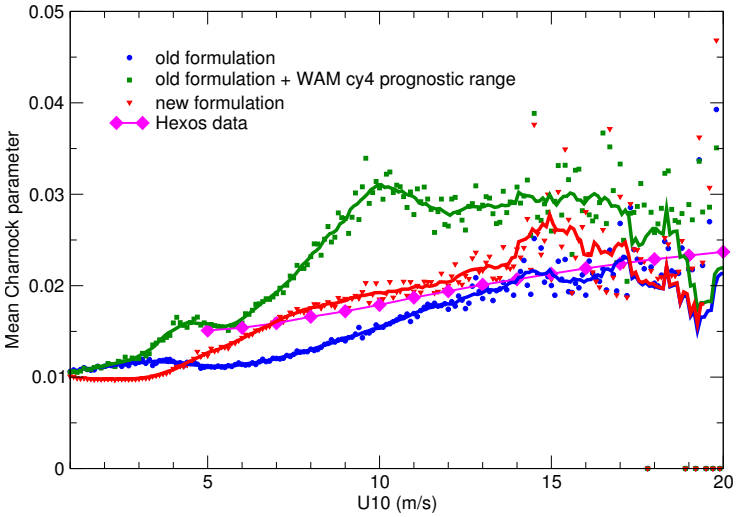

Figure 8: Typical dependence of the mean Charnock parameter on 10-m wind speed. The mean value is obtained by averaging all grid point values that are within a given $0.1\ m/s$ *wind speed bin. Solid lines are the running average of the binned data. Also shown is the relationship between the mean Charnock and the 10-m wind speed as derived from the field experiment HEXOS (Smith et al., 1992).*

4.3 Pre-operational testing

The wave model with the new formulation was tested further in a long pre-operational suite (e-suite) which also combined other modifications to the atmospheric model. Nevertheless, the impact on the wave scores was mostly determined by the new wave model and was very similar to expections from the hindcast runs (Bidlot *et al.*, 2005 a).

The operational ECWAM with the old formulation did not produce proper wave periods around India (S. Barstow, personal communication). Since October 2004, wind and wave data from buoys deployed around India available on the GTS have been processed and archived at ECMWF. Only 3 hourly data are available, nevertheless, a comparison of the operational suite (o-suite) and e-suite analyses with the data shows the remarkable improvement both in terms of wave height and mean period in the e-suite. It is clear that this positive impact is due to the new formulation as the wind speed errors do not show any change in the e-suite compared to the o-suite (even a slight degradation is suggested).

Table 3: Verification with Indian buoy data for January and February 2005. The operational model (o-suite) at the time is compared to the pre-operational model (e-suite) in terms of scatter index (standard deviation of the difference normalised by the mean of the observations) and bias (model-buoy) for wave height (H_s), mean period (T_z) and wind speed. The buoy data were obtained from the operational archive (GTS) for locations in the Arabian Sea and the Bay of Bengal (Figure 16).

Comparison with Indian buoy data : S.I.(%) [bias]		
parameter	o-suite	e-suite
H_s GTS (m)	29.2 [0.08]	26.4 [0.08]
T_z GTS (s)	29.7 [1.40]	13.8 [-0.10]
wind speed GTS (m/s)	25.6 [-0.27]	25.8 [-0.28]

5 Impact since implementation

The new formulation was implemented operationally on April 5, 2005. The impact of the change has been monitored closely. From our experience with the pre-operational testing, we believe that the improvement to the wave model since implementation is mainly due to the wave model change rather than the other changes that were made to the atmospheric model analysis and forecast system, until at least, the increase in resolution in both atmospheric (T799) and wave (40 km) models on February 1, 2006 (Untch et al., 2006).

5.1 Comparison with buoy data

Validation with buoy data confirms that since the implementation of the revised formulation, the operational wave height analysis has improved both in terms of lower scatter index and reduced bias (solid black line in Figure 9). This can be seen by comparing the last 12 months of the black solid line in Figure 9 to the previous period. The improvement is even more visible in terms of mean wave period where the date of the change is clearly visible. Also presented in Figure 9 are the results of two hindcasts of the stand-alone version of the wave model without any data assimilation. Both hindcasts are forced by 10-m wind fields from the operational analysis. The first hindcast was performed with the same model version as the operational analysis. Hence the differences with the operational analysis are due to the impact of the coupling with the atmospheric model and the use of wave data assimilation in the operational analysis. Overall, both coupling and assimilation have a beneficial impact on the quality of the analysis as can be seen from Figure 9. The second hindcast was performed with the new model version over the full extend of the run. Comparing the two hindcasts, it is clear that the new model performs better than its previous versions both in terms of wave height and mean wave period. As already noted, the mean wave period bias has become negative, but more in line with the model tendency to underestimate wind speed (Figure 9e) and wave height (Figure 9a). The new model hindcast is generally better than the operational analysis up to the point when the latter is obtained with the same model version (cycle CY31R1).

Long term comparison with 1-D wave spectra from the US and Canadian buoys is shown in Figure 10 for the operational analysis. As already anticipated from the results in Figure 7, the summer overestimation of swell energy around 12 seconds has been substantially reduced since the implementation of the new model in April 2005. Similarly, the high frequency (low period of about 6 s) part of the spectrum is in better agreement with the observations.

5.2 Comparison with ASAR

A global validation of the mean wave periods from the operational analysis with ASAR derived mean wave periods (Figure 11) in terms of bias and scatter index indicates that the old model tendency to overestimate mean wave period has been reduced with the introduction of the new model (note that the bias is defined with respect to the model in Figure 11). The scatter index has also been slightly reduced.

5.3 Forecast scores

Benefits of successive improvements to the forecasting system are nicely displayed by looking at yearly forecast scores as shown in Figure 12 for operational wave height and mean period forecasts compared to buoy data. The lastest scores are generally the best in the medium range (shown before the increase in resolution of February 2006). The latest improvements can be attributed in part to the introduction of the new model. The new setup

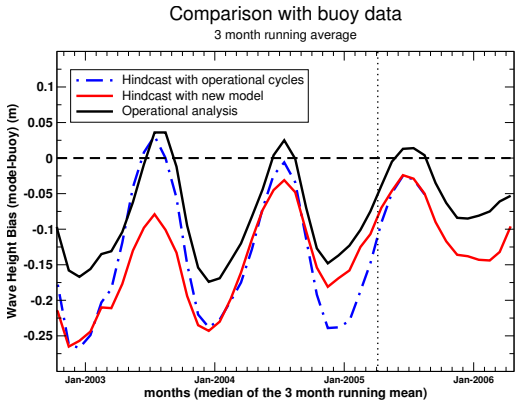

(a) wave height bias (m)

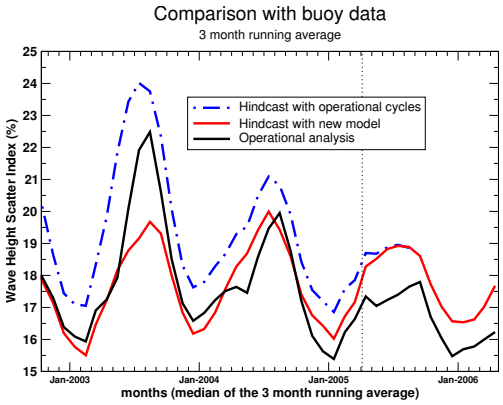

(b) wave height scatter index (%)

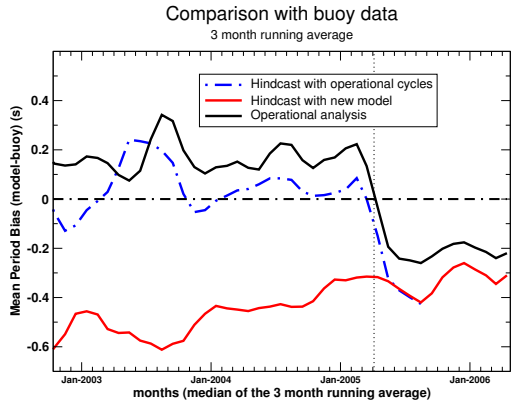

(c) mean wave period bias (s)

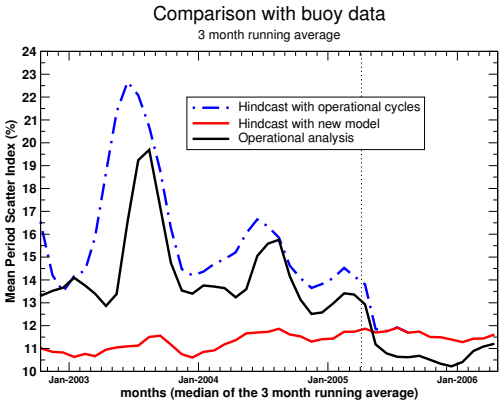

(d) mean wave period scatter index (%)

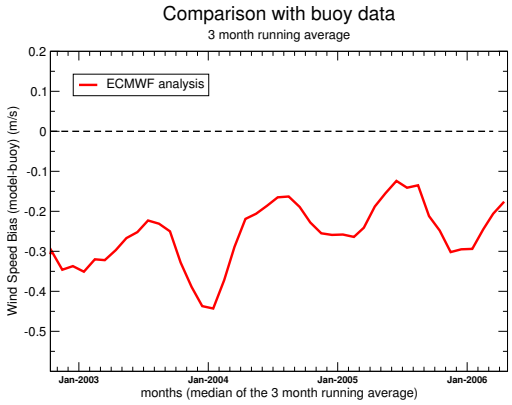

(e) wind speed bias (m/s)

Figure 9: Comparison with buoy data in terms of bias (model-buoy) and scatter index (standard deviation of the difference normalised by the mean of the observations). The operational analysis (solid black line) is compared with stand-alone 0.5° *hindcasts obtained with similar model version as operations (blue dot-dash line) and with the new model version (solid red line). The vertical dotted line indicates when the new model was introduced in operations (April 5, 2005). The statistics were computed using a 3 month running average. The comparison is presented for all selected buoy locations (Figure 16).*

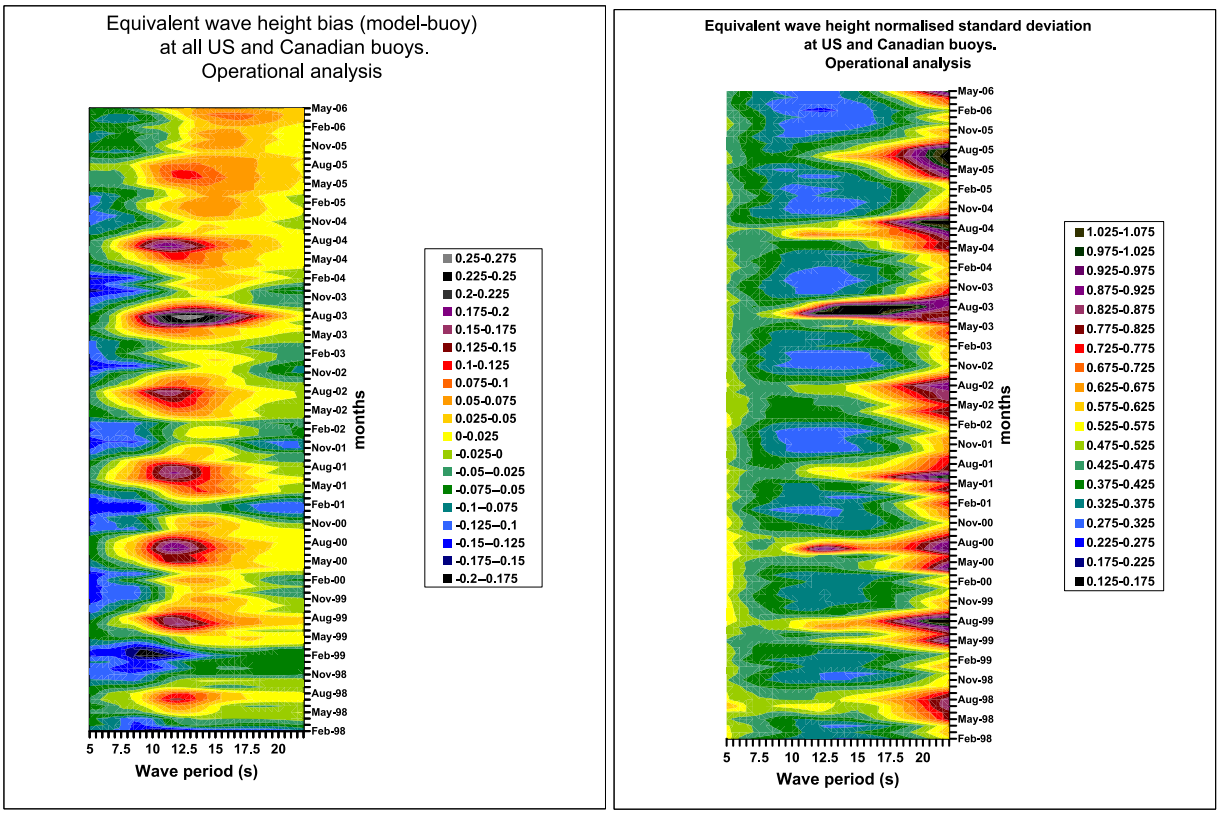

(a) equivalent wave height bias (m)

(b) equivalent wave height normalised STDEV

Figure 10: Comparison between operational wave model analysis and 1-D wave spectra for locations along the American and Canadian coasts. The spectral data were smoothed by averaging over 3 consecutive wave model frequency bins and converting the average energy density to equivalent wave heights. The different monthly statistics are then plotted in terms of the corresponding wave period of each wave model frequency bin at mid point (horizontal axis) and time (vertical axis). Normalised standard deviation of the difference (STDEV) is computed by normalising with the standard deviation of the observations for each frequency bin.

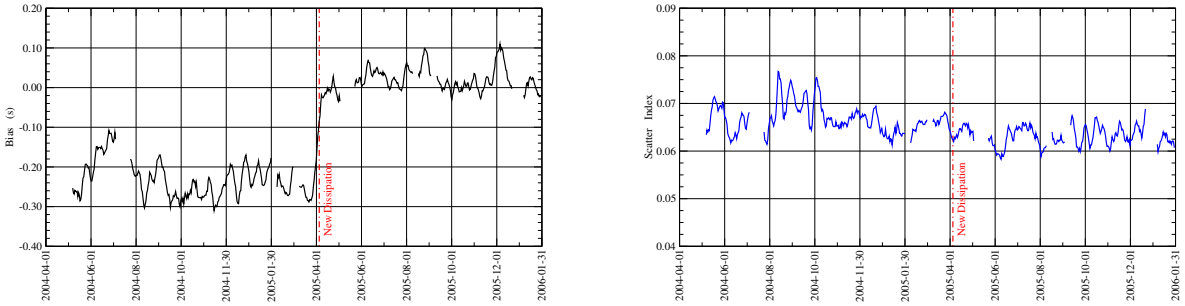

(a) Mean wave period bias (ASAR-model)

(b) Mean wave period scatter index

Figure 11: One weekly moving average of bias and scatter index of the operational analysis with respect to mean wave period derived from ENVISAT ASAR wave spectra. Bias is defined as ASAR minus model.

has a more sensitive dependence on wind speed and this explains the small degradation at later forecast ranges as also found in the pre-operational testing (Bidlot *et al.*, 2005 a). Similar conclusions follow when the standard forecast scores (i.e. against operational analysis) are produced. In particular, the Northern Hemisphere scores (Figure 13) and the Tropical scores (Figure 14) have improved considerably, while the Southern Hemisphere scores only show a small improvement (Figure 15).

6 Conclusions

On April 5, 2005, a new wave model version was implemented operationally at ECMWF. The new aspects of this model involved the reformulation of the dissipation source term in order to improve the representation of the interaction between windsea and swell. This was achieved by using an alternative definition of the mean wave number and mean frequency in the formulation for the dissipation source term thereby giving more emphasis on the high frequencies. With this new formulation of the dissipation, it was possible to relax the prognostic range of the model, resulting in a model that shows a more sensitive dependence on wind speed and wind speed error.

Pre-operational testing indicated that the impact of the new formulation and the associated changes to the wave model was positive for the wave analysis and the short range wave forecasts, especially for parameters that are more sensitive to the high frequency part of the wave spectrum such as the mean wave period.

Verification since implementation confirms the pre-operational results. Comparison of long integrations (hindcasts) of the stand-alone wave model forced by operational analysis winds shows that the latest version leads to marked improvements compared to the old model hindcasts. Furthermore, it generally gives better results than the operational analysis, which was coupled to the atmospheric model and used data assimilation. This latest wave model version will be used for the interim reanalysis. It is expected to yield a more consistent reanalysis.

7 Acknowledgements

We would like to acknowledge all wave data providers. Their data are essential in the continued development of wave models as illustrated in this paper. We are also grateful to Martin Miller for suggestions that improved the mansuscript.

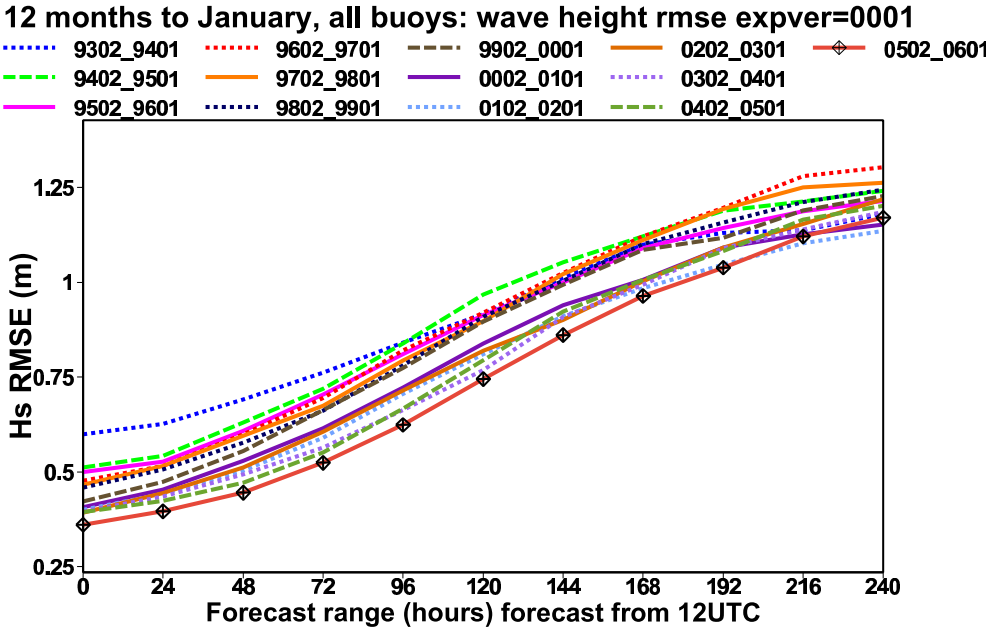

(a) Wave height RMSE (m)

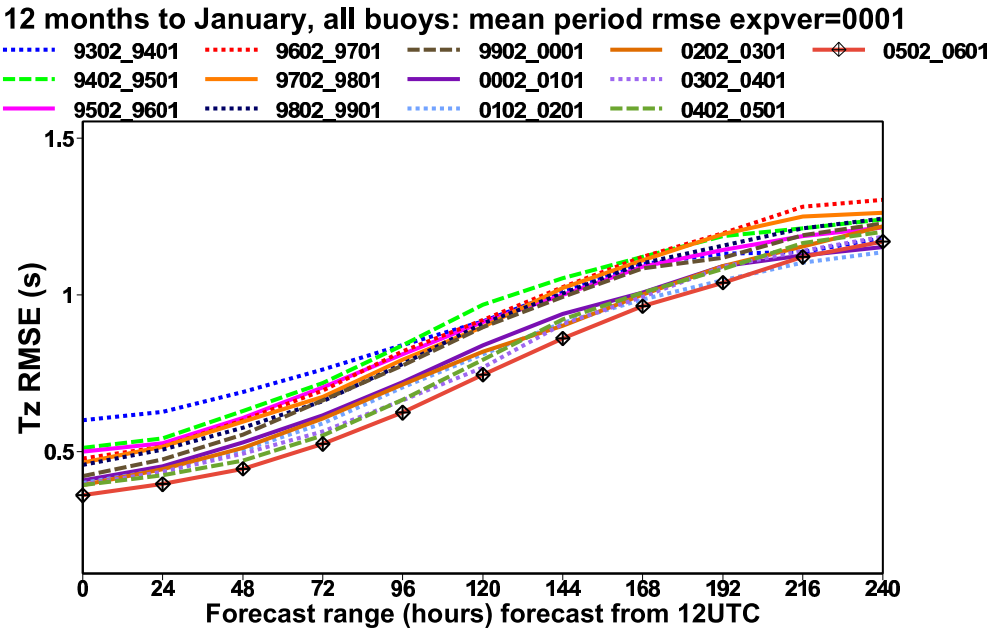

(b) Mean wave period RMSE (s)

Figure 12: Wave height (Hs) and mean wave period (Tz) forecast RMSE compared to buoy data for a full year (from February to January) since 1993. The most recent scores are displayed using a curve with diamond symbols. All forecasts from 12 UTC are used.

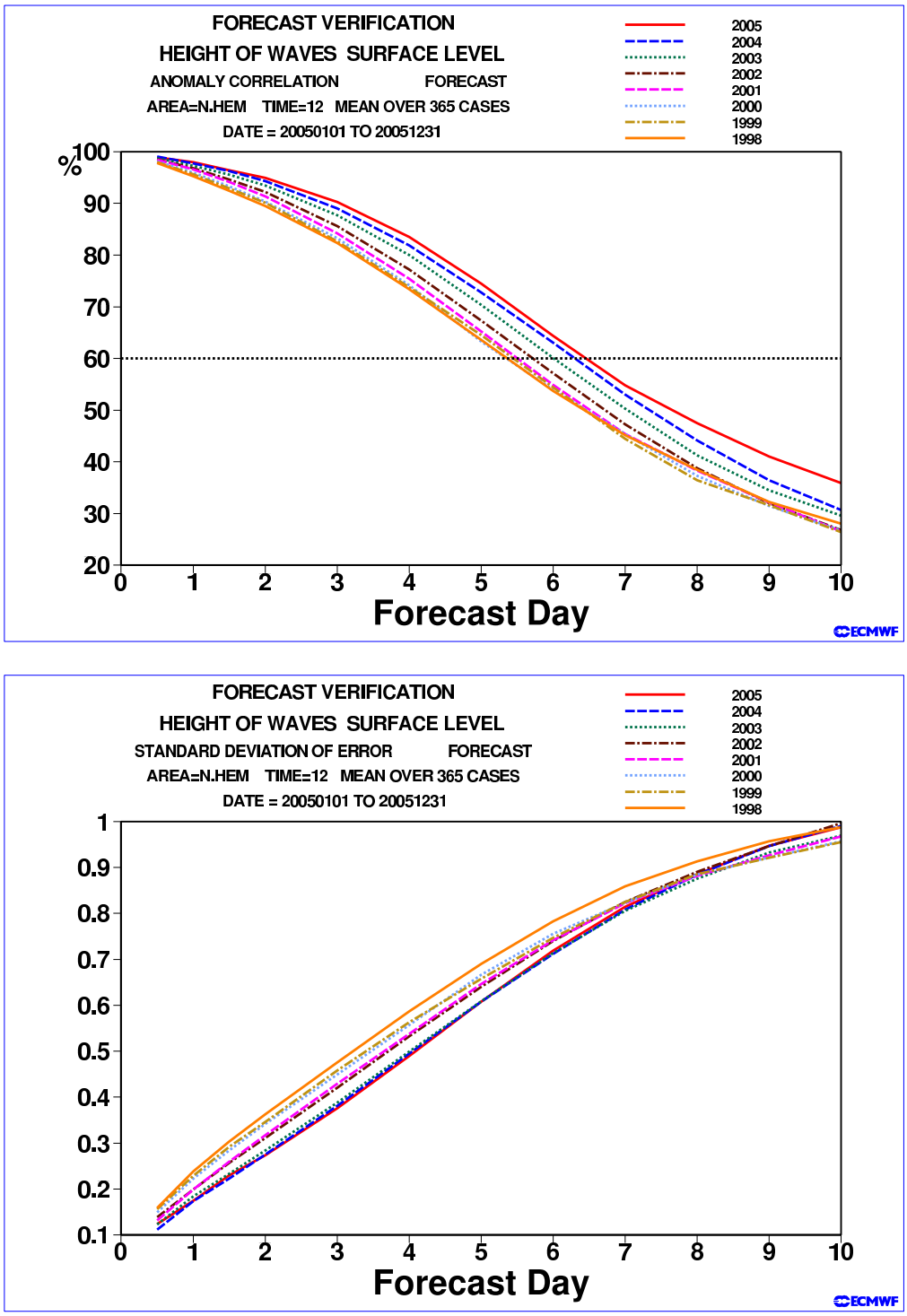

Figure 13: Northern Hemisphere wave height forecast scores compared to model analysis for a full year (from January to December) since 1998. Anomaly correlation (top panel) and standard deviation of error (bottom panel).

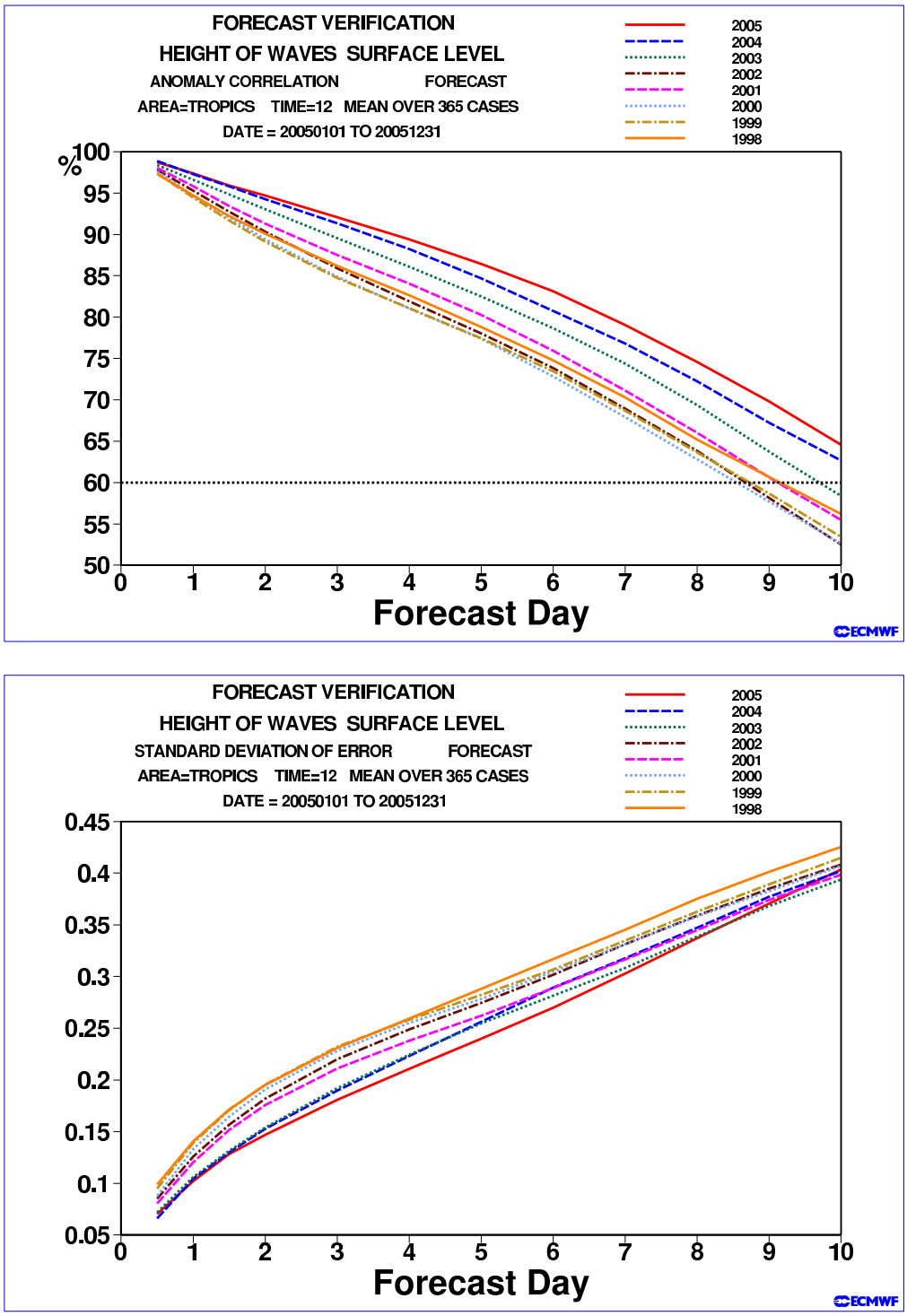

Figure 14: Tropical wave height forecast scores compared to model analysis for a full year (from January to December) since 1998. Anomaly correlation (top panel) and standard deviation of error (bottom panel).

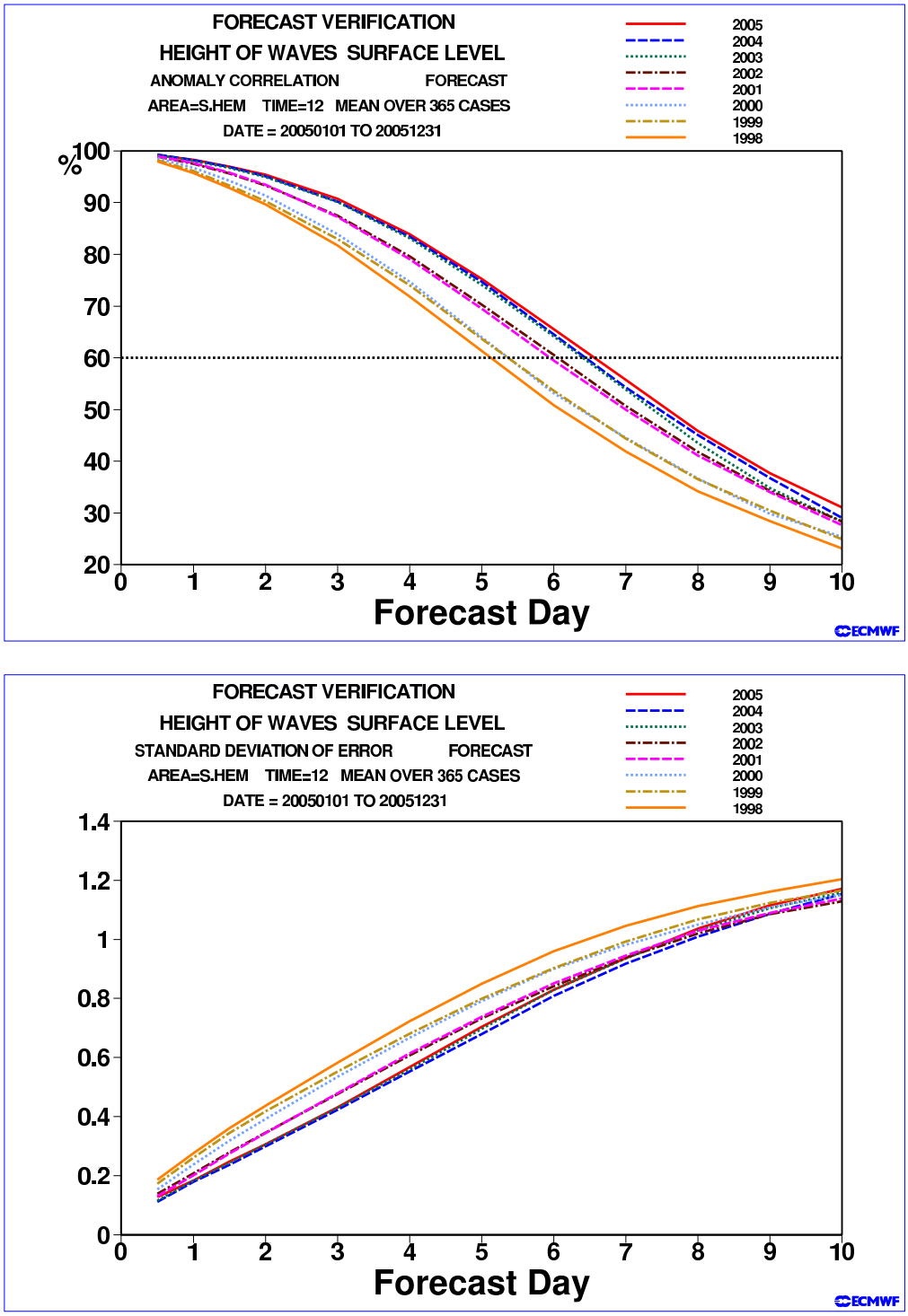

Figure 15: Southern Hemisphere wave height forecast scores compared to model analysis for a full year (from January to December) since 1998. Anomaly correlation (top panel) and standard deviation of error (bottom panel).

A Data for verifications

The different datasets used for the verifications of the different model runs are described below.

A.1 In-situ data

For years, buoy data have been used to validate wave model hindcasts. These data are usually not used by the wave data assimilation scheme and hence constitute an ideal independent data set. In-situ observations of waves are broadcasted to the meteorological community via the Global Telecommunication System (GTS). At ECMWF, most of the wave data arrive in the form of hourly SHIP data, while a small amount of data is labeled as drifting buoys (DRIBU). Most wave observations are made by dedicated meteorological buoys or specially designed wave buoys. Wave height observations from platforms and ships are also available, in particular from the North Sea area. Only significant wave height and some measure of the wave period (peak or mean) are available in the data records.

Before using the data for verification, care has to be taken to process the data to remove any erroneous observations and also in order to match the scale of both model and observations. This scale matching is achieved by averaging the hourly data in ± 2 hour time windows centered on the four major synoptic times corresponding to the normal model output times. The original quality control and averaging procedure was discussed in Bidlot *et al.* (2002). It was extended to include platform data as described in Sætra and Bidlot (2004). Note that in this paper we refer to these data as buoy data since most of them are from moored buoys, except if stated otherwise. This procedure is routinely used to assess the quality of the model wave height and period analysis and forecasts (Janssen *et al.*, 2005). The buoy networks vary with time. Overall, there has been an increase in the number of buoys with time. Figure 16 shows the locations of all buoys used in the verification for the whole of 2005. Note that valid wave data around India have only been available in the ECWMF archive since October 2004. The Australian data are actually not obtained from the ECMWF archive (i.e. not available as SHIP or DRIBU data). Rather, they are exchanged on a monthly basis with the Australian Bureau of Meteorology (BoM) when data are gathered for the operational wave model comparison as carried out informally between operational weather services with an interest in wave forecasting (Bidlot and Holt, 2006). The BoM data have only been available to us since August 2005. They are of similar quality as other GTS data.

Because the overall quality of the wind forcing has steadily improved and because of recent progress in wave modelling, a more detailed look at the wave model quality is needed. Global wave models are formulated in terms of wave spectra. Therefore the actual spectra should be validated. For a number of years now, wave spectra have become freely available for buoys along the North American Coasts. ECMWF now routinely uses 1-D spectra from those buoys to gain insight in the quality of its wave model (Bidlot *et al.* 2005 b). Buoy frequency spectra were downloaded from the NOAA National Oceanographic Data Center (NODC) and from the Canadian Marine Environmental Data Service (MEDS) web sites for respective locations shown in Figure 16. Following a basic quality check that rejects unrealistic values, hourly buoy spectra were averaged in 4-hourly time windows around the main synoptic times for which model spectra are also produced. This procedure results in more stable estimates of the spectral shape, more in line with the scale of the model spectra. Simple integration will yield traditional quantities such as significant wave height and mean wave periods. However, even more insight can be gained if model and observations are compared in terms of frequency bands. The information contained in the 1-D spectra is smoothed by integrating over frequency intervals corresponding to three consecutive wave model frequency bins and by converting the average energy density to 'equivalent' wave heights (EWH). This integration window is run across all frequency bins. The binned equivalent wave heights for the model and the buoys are compared for different frequencies or wave periods.

Note that we also show results for the comparison of the model with buoy total wave heights and mean wave periods. The hourly web data from NODC and MEDS contain these parameters (or they can be derived from the 1-D spectrum). We have therefore merged the GTS data with the web data as the latter are a bit more consistent. Furthermore, both peak and mean wave period can be produced (GTS data only contains peak period for the US and Canadian buoys). The difference in data source is represented in Figure 16 by using different symbols. Note that not all American buoys are from the web as some US buoys are not managed by NOAA.

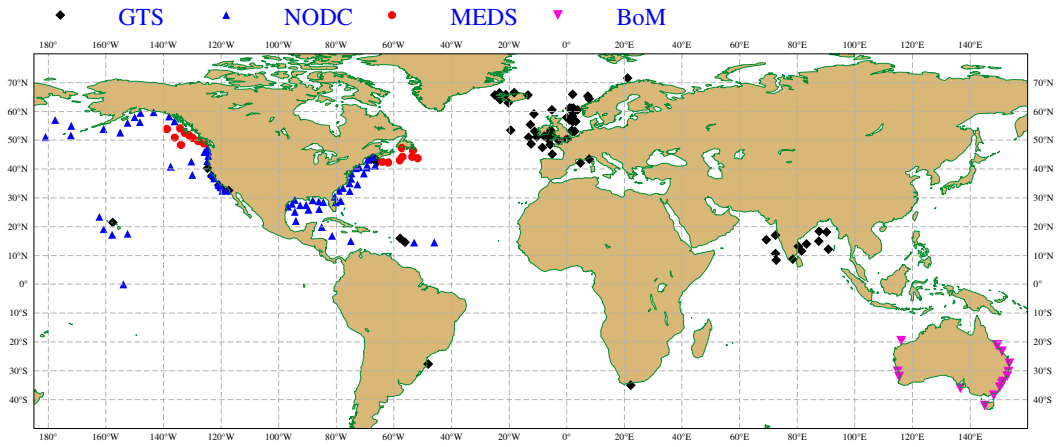

(a) buoy locations

Figure 16: Buoy locations used for the verification of 2005. The wave data were obtained from the ECMWF archive as gathered via the Global Telecomunication System (GTS), or from the web sites from NOAA National Oceanographiv Data Center (NODC) and from the Canadian Marine Environemental Data Service (MEDS), or from monthly data exchange with the Australian Bureau of Meteorology (BoM).

A.2 Radar altimeter data

Wave height can be observed from space by radar altimeter on-board several satellites. Currently, ECMWF has direct access to data from ERS-2, ENVISAT and Jason. Wave height data from ENVISAT have been assimilated operationally since the end of October 2003, replacing ERS-2, following the loss of ERS-2 global coverage in June 2003. Jason has only been recently added to the assimilation stream (Feb. 1, 2006). For verification, we will only consider ENVISAT and Jason, since ERS-2 has limited coverage and furthermore it flies over the same tracks as ENVISAT with a time difference of about 20 minutes.

Each individual altimeter observation (also referred to as the 1-Hz data) corresponds to a snapshot over a small footprint (few kilometers). Moreover, this type of observations is inherently noisy. In order to remove the obviously wrong data and to reduce the variability in the data to a level comparable to the model scale, a basic quality procedure is carried out and along track averaging is performed to create super-observations in a manner similar to what is done with buoy time series but now in space (Abdalla and Hersbach 2004). Eleven consecutive observations are averaged for ENVISAT, whereas fifteen are used for Jason.

An extensive comparison with buoy data from the beginning of both missions to present time has revealed that there is still a small residual bias in both altimeter wave height super-observations (Abdalla and Janssen, 2004, Abdalla, 2005 and Abdalla *et al.*, 2005). The comparison with buoy data was done in the context of a triple collocation excercise, in which buoy, altimeter and model wave height data are compared. The buoy data are

the same as used in the verification. The model estimates come from a long wave model hindcast which was run with the latest model version forced by 6-hourly 10-m winds from the operational analysis without any data assimilation. The altimeter data are the super observations which are assumed to be valid in the corresponding 6-hourly time window centered on the synoptic times used for buoy and model outputs.

Having 3 independent estimates of a parameter allows for the determination of both random error of each estimate and the relative bias of two of the estimates with respect to the remaining one (Janssen *et al.*, 2006). In our case, we take the buoy data as the most likely least biased data set. Another advantage of our triple collocation dataset is actually the model hindcast at both altimeter super-observation and buoy locations. The 3 datasets are first collocated based on time (within 3 hours by construct) and distance (150 km maximum separation between buoy and altimeter super-observation). The resulting collocation between altimeter and buoys is still quite scattered as 150 km and 3 hours can be a bit too large for a good fit. However, in certain cases, it might well be satisfactory. To further refine the collocation, the model hindcast can be used as a background filter. Namely, in our study, we have kept triple collocated data if the absolute difference between the model estimates at both buoy and altimeter locations normalised by the mean of both estimates is less than 5%. We have also added a check on the model mean wave direction at both locations to be within 45°. These two checks should insure that both buoys and altimeter are seeing the same wave field.

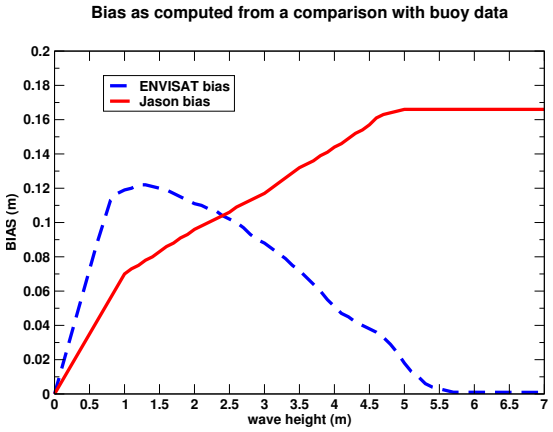

Figure 17: Altimeter wave height bias with respect to collocated buoy data. A model hindcast was used to limit the collocation error (see text). ENVISAT data were collocated with 20978 buoy observations from July 2003 to May 2006. Similarly, 28535 buoy collocations were found between October 2003 and May 2006 for Jason.

From this refined dataset, we have determined the altimeter wave height bias with respect to the buoy data by binning the collocated buoy-altimeter data both with respect to the buoys and with respect to the altimeter and by computing the average in each bin. This yields two bin averaged bias expressions as a function of wave height. Since both buoy and altimeter observations have errors, an estimate of the bias is then computed by taking the average of these 2 expressions. Figure 17 shows the resulting bias for both ENVISAT and Jason with respect to the buoy data. We have assumed that these bias estimates are valid globally and have substracted them from the altimeter super-observations when comparing model hindcasts.

A.3 ASAR data

Radar altimeter only yields significant wave heights and wind speeds over a small footprint. A more detailed description of the sea state requires the full two- dimensional wave energy spectrum. Such observations, albeit

neither necessarily fully comprehensive nor independent, are already available from the ERS-2 synthetic aperture radar (SAR) and from the ENVISAT advanced SAR (ASAR). The latter has higher spectral resolution and operates at twice the nominal ERS data coverage by providing data every 100 km along the satellite track over the oceans. ERS-2 SAR is not considered here due to the dominance of ENVISAT coverage.

Spectra as derived from the ENVISAT ASAR wave mode imagette spectra are processed operationally to retrieve ocean wave spectra using an inversion scheme based on the work done by Hasselmann *et al.* (1996). The inversion scheme relies on a model first guess to resolve the directional ambiguity and to provide first guess information on the wave spectrum. A basic quality check of the data is done (Abdalla and Hersbach, 2004). Integrated parameters such as significant wave height and mean wave period can be derived from the inverted spectra and compared to the model. Note that ENVISAT ASAR wave model level 1b data have been assimilated in the operational model since February 1, 2006.

References

Abdalla, S., 2005: Global validation of ENVISAT wind and water vapour products from RA-2, MWR, ASAR and MERIS, *Contract Report to the European Space Agency*, December 2005, 75pp.

Abdalla, S., P. Janssen, and J.-R. Bidlot, 2003: Use of satellite data and enhanced physics to improve wave prediction. *28th International Conference on Coastal Engineering*, Cardiff July 2002, Word Scientific Publishing.

Abdalla, S. and H. Hersbach, 2004: The technical support for global validation of ERS wind and wave products at ECMWF. *Final Report for ESA contract* 15988/02/I-LG, ECMWF, Shinfield Park, Reading, U.K., 46pp. Available online at: http://www.ecmwf.int/publications/

Abdalla, S., and P. Janssen, 2004: Global validation of ENVISAT RA-2 wind and wave, and MWR products. *Proc. ENVISAT-ERS Symposium*, Salzburg, Austria, 6-10 Sep. 2004.

Abdalla, S., Bidlot, J. and Janssen, P., 2005: Jason altimeter wave height verification and assimilation, In: Ozhan, E. (Editor), *Proc. Seventh International Conference on the Mediterranean Coastal Environment (MEDCOAST 05)*, Kusadasi, Turkey, 25-29 Oct. 2005, 1179-1185.

Ardhuin, F., 2005: Etat de la mer et dynamique de l'océan superficiel. *Mémoire d'habilitation à diriger des recherches*, Université de Bretagne Occidentale, Best, France.

Ardhuin, F., T.H.C. Herbers, G.Ph. van Vledder, K.P. Watts, R. Jensen, and H.C. Graber, 2007: Swell and slanting fetch effects on wind wave growth. paper in press in *J. Phys. Oceanogr.*.

Bidlot J.-R., D. J. Holmes, P. A. Wittmann, R. Lalbeharry, H. S. Chen, 2002: Intercomparison of the performance of operational ocean wave forecasting systems with buoy data. *Wea. Forecasting*, **17**, 287-310.

Bidlot, J., B. Hansen and P. Janssen, 1999: Improved representation of stress and mean square slope. *Internal Memorandum Research Department* R60.9/PJ/54. ECMWF, Reading, U.K., available from authors upon request.

Bidlot, J. and P. Janssen, 2003: Unresolved bathymetry, neutral winds and new stress tables in WAM (main contribution to CY28R1). *Internal Memorandum Research Department* R60.9/JR/0400. ECMWF, Reading, U.K., available from authors upon request.

Bidlot, J., P. Janssen, and S. Abdalla, 2005 a: A revised formulation for ocean wave dissipation in CY29R1. *Internal Memorandum Research Department* R60.9/JR/0516. ECMWF, Reading, U.K., available from authors upon request.

Bidlot J.-R., P.A.E.M. Janssen, and S. Abdalla, 2005 b: On the importance of spectral wave observations in the continued development of global wave models. *Proc. Fifth Int. Symposium on Ocean Wave Measurement and Analysis WAVES2005*, 3rd-7th July 2005, Madrid, Spain.

Bidlot J.-R. and M.W. Holt, 2006: Verification of operational global and regional wave forecasting systems against measurements from moored buoys. *JCOMM Technical Report*, **30**. WMO/TD-No. 1333.

Booij, N. and L. Holthuijsen, 2002: The effect of swell and wave steepness on the wave growth and depth-induced wave breaking. *Proc. 7th International Workshop on Wave Forecasting and Hindcasting*, Banff, Alberta, Canada.

Hasselmann, K., 1974: On the spectral dissipation of ocean waves due to whitecapping. *Boundary Layer Meteorol.* **6**, 107-127.

Hasselmann S., C. Brüning, K. Hasselmann, and P. Heimbach, 1996: An improved algorithm for the retrieval of ocean wave spectra from SAR image spectra. *J. Geophys. Res.*, **101**, C7, 16615- 16629.

Hersbach, H. and P.A.E.M. Janssen, 1999: Improvement of the short-fetch behavior in the wave ocean model (WAM). *J. Atm. Ocean. Techn.*, **16**, 884-892.

Janssen, P. 2004: *The Interaction of Ocean Waves and Wind*. Cambridge University Press, 300pp.

Janssen, P. and J. Bidlot, 2001: Impact of revised surface roughness calculation on mini vorticices (CY24R2). *Internal Memorandum Research Department* R60.9/PJ/44. ECMWF, Reading, U.K., available from authors upon request.

Janssen P.A.E.M., S. Abdalla, H. Hersbach, and J.-R. Bidlot 2006: Error estimation of buoy, satellite and model wave height data. accepted for publication in *J. Atm. Ocean. Techn.*.

Janssen P, J.-R. Bidlot, S. Abdalla and H. Hersbach, 2005: Progress in ocean wave forecasting at ECMWF. *ECMWF Tech. Memo.*, **478**. ECMWF, Reading, U.K., 27 pp., available online at: http://www.ecmwf.int/publications/

Komen, G.J., K. Hasselmann and S. Hasselmann, 1984: On the existence of a fully developed windsea spectrum. *J. Phys. Oceanogr.*, **14**, 1271-1285.

Komen, G.J., L. Cavaleri, M. Donelan, K. Hasselmann, S. Hasselmann, and P.A.E.M. Janssen, 1994: *Dynamics and Modelling of Ocean Waves*. Cambridge University Press, 554pp.

Kraan, C., W.A. Oost and P.A.E.M. Janssen, 1996: Wave energy dissipation by whitecaps. *J. Atmos. Oceanic Technol.*, **13**, 262-267.

Kumar, R., D. Stammer, W.K. Melville, and P. Janssen, 2003: Electromagnetic bias estimates based on TOPEX, buoy, and wave model data. *J. Geophys. Research*, **108**, 3351, doi:10.1029/2002JC001525.

Lafon C., Piazzola J., Forget P., Le Calve O., Despiau S., 2004: Analysis of the variations of the whitecap fraction as measured in a coastal zone. *Boundary Layer Meteorol.*, **111**, 229-360.

Osuna P., A.J. Souza and J. Wolf, 2006: Effect of deep-water wave breaking dissipation on the wind-wave modelling in the Irish Sea. *Journal of Marine System*, doi:10.1016/j.jmarsys.2006.09.003.

Pierson, W.J.,Jr and L. Moskowitz, 1964: A proposed spectral form for fully developed wind seas based on the similarity theory of S.A. Kitaigorodskii. *J. Geophys. Res.*, **69**, 5181.

Sætra, Ø. and J.-R. Bidlot, 2004: On the potential benefit of using probabilistic forecast for waves and marine winds based on the ECMWF ensemble prediction system. *Wea. Forecasting*, **19**, 673-689.

Smith, S.D., R.J. Anderson, W.A. Oost, C. Kraan, N. Maat, J. DeCosmo, K.B. Katsaros, K.L. Davidson, K.

Bumke, L. Hasse and H.M. Chadwick, 1992: Sea surface wind stress and drag coefficients: the HEXOS results. *Boundary Layer Meteorol.*, **60**, 106-142.

Snyder, R.L., F.W. Dobson, J.A. Elliott and R.B. Long, 1981: Array measurements of atmospheric pressure fluctuations above surface gravity waves. *J. Fluid Mech.*, **102**, 1-59.

Tolman, H. and D. Chalikov, 1996: Source terms in a third-generation wind wave model. *J. Phys. Oceanogr.*, **26**, 2497-2518.

Untch A., M. Miller, M. Hortal, R. Buizza, and P. Janssen, 2006: Towards a global meso-scale model: The high-resolution system T799L91 and T299L62 EPS. *ECMWF Newsletter*, **108**, 6-13. ECMWF, Reading, U.K, available online at: http://www.ecmwf.int/publications/

Young I.R. and A.V. Babanin, 2006: Spectral distribution of energy dissipation of wind-generated waves due to dominant wave breaking. *J. Phys. Oceanogr.*, **36**, 376-394.